ASSOCIAZIONE NAZIONALE ITALIANA DI INGEGNERIA SISMICA
ANIDIS
Italian National Association of Earthquake Engineering

XVIII CONVEGNO ANIDIS
L'ingegneria sismica in Italia
ASCOLI PICENO 2019
15-19 Settembre

Experimental tests of unreinforced external RC beam-column joints strengthened with prestressed steel strips

Gerardo M. Verderame[a], Paolo Ricci[a], Maria Teresa De Risi[a], Carlo Del Gaudio[a], Alessandro Vari[b], Marianna Leonori[b]

[a] *Department of Structures for Engineering and Architecture, University of Naples Federico II, Via Claudio 21, 80125 Naples, Italy*

[b] *EDIL CAM® Sistemi Srl, Via dei Genieri 39, 00143 Rome, Italy*

Keywords: reinforced concrete beam-column joints; experimental; strengthening; prestressed steel strips; CAM® technology

ABSTRACT

The response of unreinforced beam-column joints represents a key issue in seismic vulnerability and fragility assessment of existing Reinforced Concrete (RC) buildings. Within this framework, a great attention is focused on the investigation of the experimental response of unreinforced joints strengthened with different technologies, based on traditional or innovative materials, and with different complexity/cost. In this study, an experimental investigation of the response of external RC beam-column joints is presented. Four specimens are tested, namely one as-built, unreinforced (without stirrups in the joint panel region) specimen, one reinforced with a code-compliant amount of transverse reinforcement (stirrups) in the joint panel – for reference and comparison purposes, and two specimens strengthened with the application of prestressed steel strips as external transverse reinforcement, using the CAM® technology with two different layouts characterized by a different complexity of installation. The response of the unreinforced specimen was controlled by joint panel failure following beam yielding, whereas the specimen reinforced with code-compliant joint stirrups showed a ductile behaviour, controlled by beam flexural failure. The response of the strengthened specimens demonstrated the effectiveness of the adopted technology, that led to a ductile response – as for the specimen reinforced with stirrups – or to a joint panel failure following beam yielding – as for the as-built unreinforced specimen, but with a higher global ductility. The experimental results are reported and discussed, in terms of global response of the sub-assemblage and of observed damage evolution, and in terms of local response, such as shear distortion of the joint panel and measured strain of strengthening steel strips. The effectiveness of the tested strengthening solutions is evaluated through a comparison with the response of the reference (as-built unreinforced and reinforced with code-compliant joint stirrups) specimens.

1 INTRODUCTION

Within the very wide and complex research field regarding the seismic assessment and strengthening of Reinforced Concrete (RC) existing buildings, the response of unreinforced (i.e. without transverse reinforcement in the joint panel) beam-column joints plays a key role, as demonstrated by post-earthquake damage observation (e.g. Ricci et al., 2011). Moreover, there are several issues still under scientific investigation, regarding the assessment of the experimental response (e.g., Clyde et al., 2000; Pantelides et al., 2002; Wong, 2005; Masi et al., 2013; De Risi et al., 2016; Ricci et al., 2016, De Risi and Verderame, 2017), the development of capacity models (e.g., Park and Mosalam, 2012; Jeon et al., 2014), the modelling of the nonlinear response (Celik and Ellingwood, 2008, Jeon et al., 2015; De Risi et al., 2017; De Risi et al., 2018), and the design of strengthening interventions for these elements. Regarding the latter issue, more specifically, apart from the approaches based, for instance, on RC jacketing (e.g. Karayannis et al., 2008), which increases also the joint resisting area, several approaches have been developed aimed at compensating the lack of transverse reinforcement with added tension-resistant materials. Within these approaches, two main types of technologies have been applied, namely one based on composite

materials, for which several studies, especially experimental-based, are present in the scientific literature (e.g., Thermou and Elnashai, 2006; Antonopoulos and Triantafillou, 2003; Del Vecchio et al., 2014), and one based on more "traditional" materials/techniques, typically employing steel elements (e.g. Shafaei et al., 2014; Yurdakul and Avsar, 2016). The design of the strengthening intervention and its effectiveness clearly depend on the expected failure mode of the unreinforced joint, too (e.g., J-, BJ- or CJ-failure, respectively prior to yielding of adjoining members, following flexural beam yielding and following flexural column yielding).

In this study, the results of experimental tests on unreinforced external RC beam-column joints strengthened with the CAM® technology are presented. This strengthening method is based on the use of prestressed steel strips, providing confinement and added tension resistance to unreinforced or, more generally, "deficient" structural elements; it was originally developed for the seismic strengthening of unreinforced masonry buildings, but was successfully adopted also for RC existing buildings (Dolce et al., 2001a,b; Spinella et al., 2014). More specifically, a very similar strengthening technique for unreinforced RC beam-column joints, compared to this study, was recently presented by Yang et al. (2019).

Results of experimental tests on unreinforced external RC beam-column joints are presented, representative of an existing, non-ductile RC building, strengthened with two different versions of application of the CAM® technology, and, as a reference for comparison purposes, on two identical specimens, one as-built (without strengthening) and another one reinforced with code-compliant transverse reinforcement in the joint panel. The as-built, unreinforced specimen shows a joint panel failure following beam yielding. The analysis of experimental data regarding the global and local response of the strengthened specimens shows the effectiveness of the adopted strengthening solutions, also compared to the code-compliant reinforced specimen.

In the following, the experimental program is illustrated first, reporting the description of the specimens, the design and application process of the adopted strengthening technologies, the setup and instrumentation layout and the loading protocol. Then, experimental results are described, illustrating the global response and damage evolution, and the local response in terms of joint panel response and measured strains in beam longitudinal reinforcement and joint panel reinforcement, if present (i.e., stirrups or external steel strips), and results are discussed.

2 EXPERIMENTAL PROGRAM

In this Section, the tested specimens, the instrumentation layout and the testing procedure are described.

2.1 Specimens

The specimens were designed in order to be representative of full-scale external RC beam-column joints of an existing three-storey building designed for moderate seismic loads according to past Italian technical codes (D.M. 1986; D.M. 1992). The geometry of the specimens reproduces an interstorey height equal to 3.4 m (L_c=3.4/2=1.7 m) and a bay length equal to 3.6 m (L_b=3.6/2=1.8 m), with L_c and L_b intended to represent the shear span of column and beam elements, respectively. A "short transverse beam" (35 cm long) was added, to provide confinement to the other internal side of the joint panel, aimed at reproducing the effect of the presence of a beam in transverse direction, too. Geometry and reinforcement details (specifically, with reference to the specimen with stirrups in the joint panel) are reported in Figure 1.

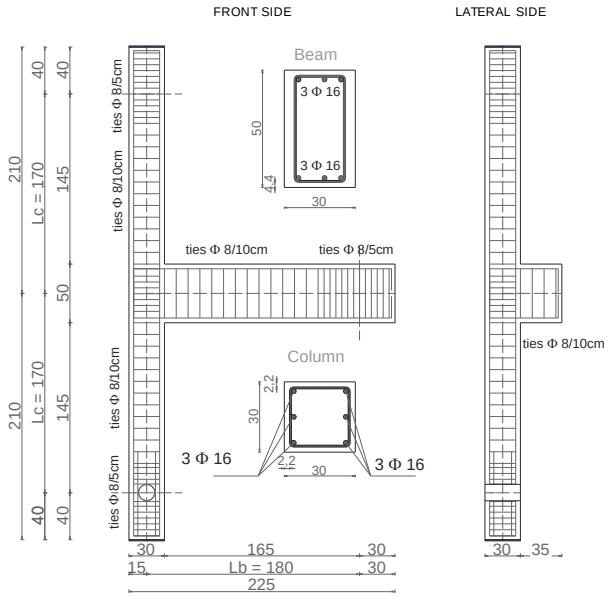

Figure 1. Geometry and reinforcement details (of the specimen with stirrups in the joint panel).

Beam's and column's section are (30×50) cm^2 and (30×30) cm^2, respectively, with longitudinal reinforcement made of (3+3) 16 mm bars in both cases. The clear length of beam and columns is therefore equal to L'_b=1.8-0.15=1.65 m and L'_c=1.7-0.25=1.45 m, respectively. The code-compliant (NTC 2008) transverse reinforcement in the joint panel in the "S" specimen consists of

8 mm stirrups spaced at 50 mm. The remaining specimens (as-built unreinforced, "NS"; strengthened with first solution of CAM® technology, "CAM1"; strengthened with second solution of CAM® technology, "CAM2") have no transverse reinforcement in the joint panel.

The mean concrete cylindrical compressive strength (f_c) is equal to 32.2 MPa. The yield (f_y) and ultimate (f_t) strength of reinforcing steel is equal to 503 MPa and 627 MPa for 16 mm diameter bars used as longitudinal reinforcement and 460 MPa and 541 MPa for 8 mm diameter bars used as transverse reinforcement, respectively.

(a)

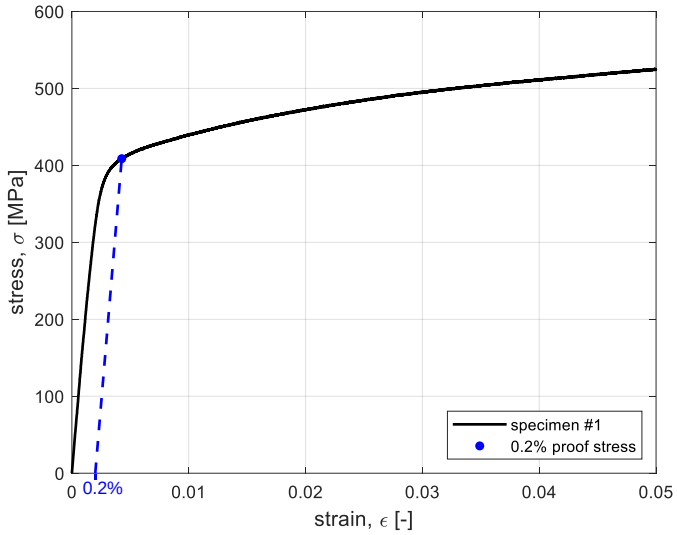

(b)

Figure 2. Photographic image of a tensile test (a) and obtained stress-strain relationship (b) of a steel strip used for CAM® strengthening.

The steel strips used for CAM® strengthening have a (A_{strips} =) 19×0.9 mm^2 transverse section. The stress-strain constitutive relationship obtained from tensile test is reported in Figure 2. The stress-strain response is similar to the typical response of a cold worked steel. Hence, the 0.2% proof stress (CEN, 2004) is evaluated, instead of the yield stress, and it is equal to $f_{0.2}$ = 409 MPa. The initial elastic modulus is equal to 180 GPa. The tensile stress actually applicable to the steel strips in the prestressing installation phase is limited by mechanical equipment issues to f_p = 120 MPa.

Two main approaches can be used for the design of the intervention (Leonori and Vari, 2019):

- A "prestress-based" approach, in which the horizontal stress due to the active confinement provided by the prestressed steel strips, combined with the vertical stress acting on the joint core due to the axial load in the column and with the shear stress due to the joint shear, is able to limit the principal tensile stress, compatible with the concrete tensile strength. This approach is consistent with the principal stress-based approach usually adopted for beam-column joints without transverse reinforcement (Priestley, 1997).
- A "transverse reinforcement" approach, in which the contribution of the steel strips is taken into account as an added transverse reinforcement, and the formulations used for designing the amount of stirrups in joint panel in new buildings are adopted.

Both of these approaches are consistent with the provisions of the Italian technical code (NTC 2008, 2018; Circolare 2009, 2019) and of Eurocode 8-part 1 and part 3 (CEN, 2005a,b).

In order to design the strengthening intervention, independent of the adopted type of approach, the joint shear demand has to be evaluated. To this end, adopting a simplified

2.2 Design of strengthening

CAM® technology is based on the use of closed prestressed steel strips installed through transverse holes realized in structural elements, providing active confinement and tension resistance to the deficient structural member to be strengthened.

In the case of unreinforced RC beam-column joints, the application of the CAM® technology consists of the installation of the closed prestressed steel strips around the unreinforced joint panel, completely similar to "externally added" stirrups.

code-based approach, the flexural strength of beam and column is evaluated with a parabola-rectangle constitutive relationship for concrete in compression and an elastic-perfectly plastic constitutive relationship for reinforcing steel, adopting mean values for material properties. A constant axial load equal to N_c = 290 kN is applied to the column, corresponding to an axial load ratio ν=0.10. The resulting expected values of flexural strength at yielding and maximum for beam and column are $M_{b,y}$ = 123 kNm, $M_{b,max}$ = 131 kNm, $M_{c,y}$ = 102 kNm, and $M_{c,max}$ = 106 kNm, respectively, leading to a weak beam-strong column hierarchy, with the attainment of beam's maximum flexural strength expected prior to columns' yielding, being $(2 \cdot M_{c,y}) > M_{b,max}$.

Within the second approach, the following formulation can be adopted, using, again, mean values of the material properties:

$$\sigma_{jh}\left(=\frac{n_{strips}\left(2A_{strips}\right)f_{0.2}}{A_{jv}}\right)\geq\frac{\tau_j^2}{f_{ct}+\sigma_{jv}}-f_{ct} \qquad (1)$$

with A_{jv} representing the vertical joint area. The joint shear stress, τ_j, is calculated as the ratio between the horizontal joint shear, V_{jh}, and the horizontal joint area, A_{jh}. From simple equilibrium considerations, V_{jh} is calculated as:

$$V_{jh}=T-V_c=T-\frac{V_b L_b}{2L_c} \qquad (2)$$

with T representing the tension in beam longitudinal reinforcement, and V_c the column shear. The V_{jh} value for designing the strengthening can be evaluated starting from the maximum expected tension in beam longitudinal reinforcement ($T = A_{s,b} \cdot f_y$) and the beam shear corresponding to the maximum flexural strength ($V_b = M_{b,max}/L'_b$). The axial load in the column has to be referred to the most unfavourable condition, i.e. diminished by the beam shear corresponding to the maximum flexural strength ($N_{jv} = N_c - V_b$) (see the static scheme reported in Figure 4). The concrete tensile strength in Eq. (1) has been assumed equal to $f_{ct} = 0.30 \cdot f_c^{0.5}$ = 1.70 MPa, for consistency and simplicity equal to the value of concrete tensile strength that should be employed adopting the principal stress-based approach proposed for unreinforced joints by the Italian code (Circolare 2009, 2019), and very close to the corresponding value proposed by Priestley (1997), i.e. $0.29 \cdot f_c^{0.5}$.

Evaluating under these assumptions the joint shear ($\tau_j = V_{jh}/A_{jh}$) and vertical normal ($\sigma_{jv} = N_{jv}/A_{jh}$) stress, the necessary horizontal normal stress, σ_{jh}, is obtained from Eq. (1), equal to 1.52 MPa.

The steel strips were arranged in three layers, along the height of beam, as reported in Figure 3. The minimum number of strips in each layer can be calculated starting from the calculated necessary horizontal normal stress, σ_{jh}, the transverse section area of each strip, A_{strips}, and the $f_{0.2}$ stress, thus obtaining a number of strips at each layer, n_{strips}, equal to 4.1, which is rounded to five. Note that in Eq. (1) the area of each strip, A_{strips}, is multiplied by 2 in order to take into account the presence of two ties for each strip.

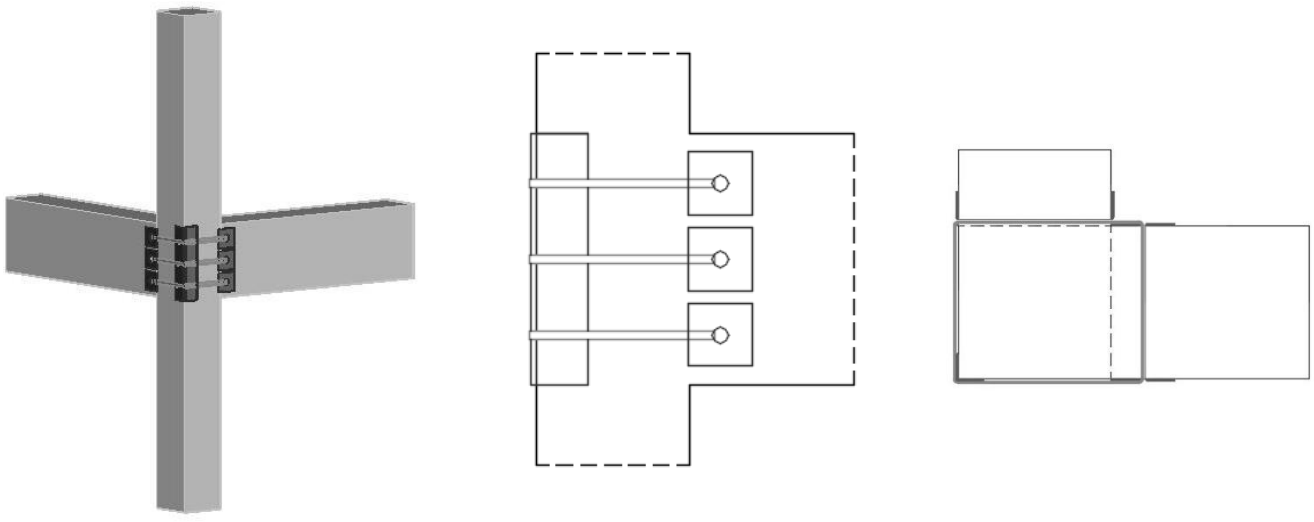

(a) (b) (c)

Figure 3. 3D (a), side (b) and top (c) view of the strengthening layout for CAM1 test.

It is possible to evaluate if the adopted strengthening layout could satisfy also the first design approach described above, i.e. if cracking in the joint panel should be prevented or not under the prestress action. Note that, indeed, evaluating the principal tensile stress under the

effect of the initially prestressed steel strips, and comparing it with the concrete tensile strength, is the same as applying Eq. (1) with a tensile stress in the strips equal to f_p instead of $f_{0.2}$, and, clearly, more strictly. As expected, such a verification according to the first approach would not be satisfied, see Figure 4, i.e. cracking in the joint panel is anyway expected, also in the strengthened specimen.

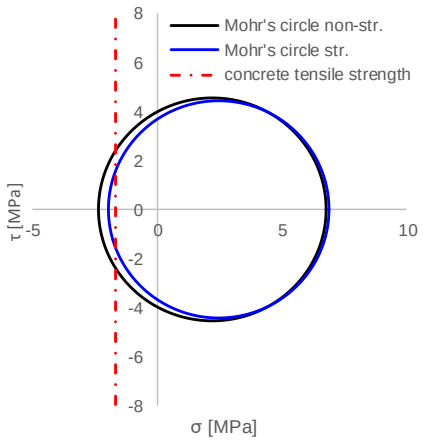

Figure 4. Mohr's circle for concrete in the joint panel for the non-strengthened (black) and strengthened (blue) specimens, with the principal tensile stress exceeding (in both cases) the concrete tensile strength.

As an alternative to the strengthening solution adopted for "CAM1" test, a further possible layout was investigated, named "CAM2": in order to evaluate the effectiveness of a less invasive solution, the transverse holes passing through the beams (i.e., the beam in the plan of the subassemblage and the transverse short beam) were replaced by a single, diagonal, 45-degree inclined hole directly connecting beams' external faces and passing through the joint core (see Figure 5). Such a kind of solution could be applied avoiding the refurbishment of internal, non-structural finishing elements, such as plaster layers (on beams' internal sides), thus ensuring significant advantages in monetary and functional terms.

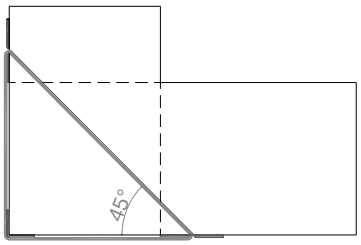

Figure 5. Top view of the strengthening layout for CAM2 test.

2.3 Setup and loading protocol

The experimental setup reproduces the static scheme reported in Figure 6a, statically determined, with a hinge and a roller at the two half columns' ends, corresponding to the theorical points of contraflexure at mid-storey height, with the hydraulic actuator at beam's end, at the same point. A hydraulic jack applies to the column a constant axial load equal to 290 kN, corresponding to an axial load ratio ν=0.10. The hydraulic actuator at beam's end imposes a cyclic displacement path corresponding to the drift protocol reported in Figure 6b, with the drift calculated as the ratio between the displacement imposed at beam's end and the beam's length, with three sub-cycles for each maximum imposed drift value.

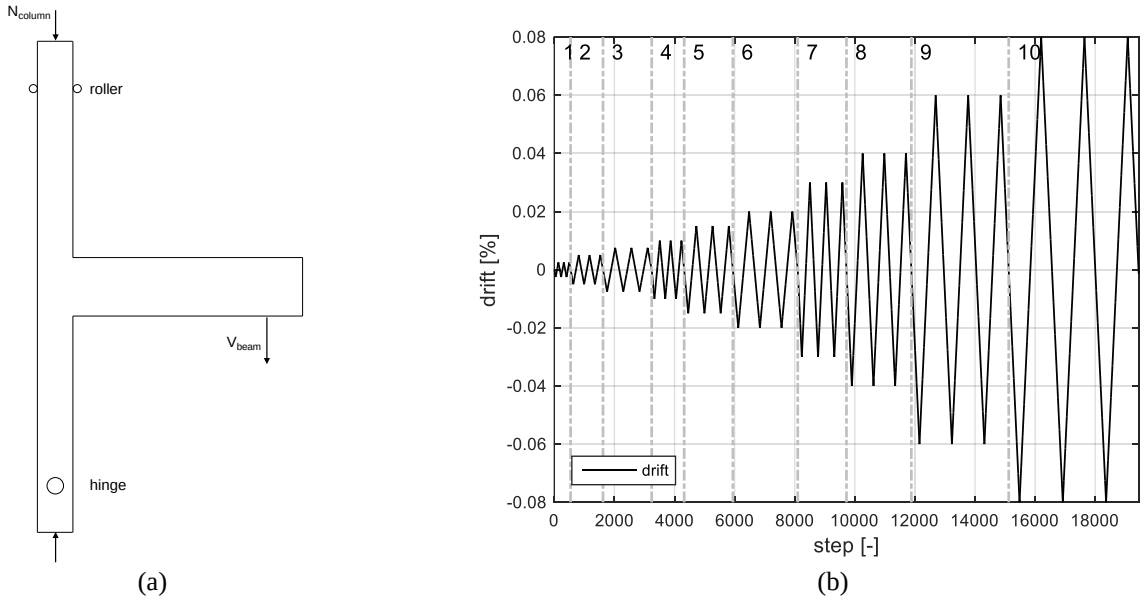

(a) (b)

Figure 6. Schematic setup representation (a) and imposed drift protocol (b).

Note that very slight differences can be observed between the displacement theoretically imposed by the hydraulic actuator and the displacement actually measured at beam's end, due to deformability of setup elements, resulting in actual drift values slightly lower than the reference values reported in Figure 6b and, later, in Tables 1 and 2.

Ten Linear Potentiometers (LPs) were used to measure the joint shear strain (located along the longitudinal reinforcement layers of beam and column and along the diagonals of the joint panel) and the fixed-end-rotation in column, at the interface with the joint panel (located along the longitudinal reinforcement layers). Similarly, two Linear Variable Displacement Transducers (LVDTs) were used to measure the fixed-end-rotation in beam, at the interface with the joint panel (located along the longitudinal reinforcement layers). Two further LVDTs at beam's end were used in strengthened specimens, in order to measure the crack width along two different end beam's portions, including or not the transverse holes used for steel strips (see Section 2.2). Further LVDTs were used to measure the rotation at top and bottom columns' ends and at the external joint's face. Finally, a wire potentiometer was used to measure the beam's end displacement.

In each specimen, two strain gauges were used to measure the bar strain in top and bottom beam's longitudinal reinforcement layers, at the interface section with the joint panel. In the "S" specimen, a strain gauge was used to measure the strain in the mid-height stirrup located in the joint panel, too. In strengthened specimens, six strain gauges were used to measure the strain in the prestressed steel strips, i.e. two per each layer, one on the first (inner) strip and one on the fifth (outer) strip.

A schematic of the main LPs, LVTDs and strain gauges used to measure the data analysed in the following is reported in Figure 7.

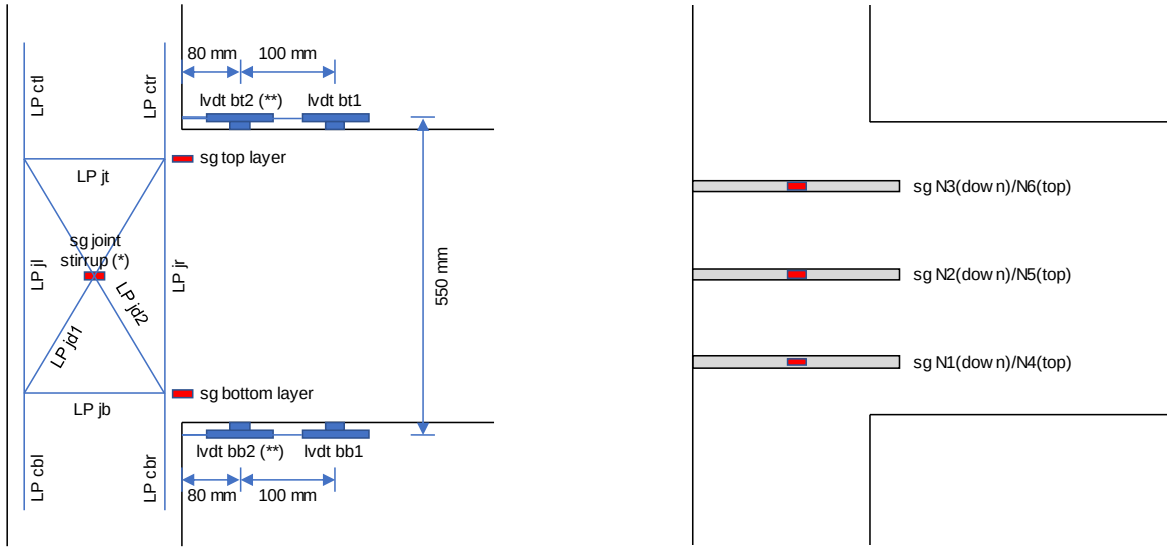

(a) (b)

(*): present only in "S" specimen; (**) present only in "CAM1" and "CAM2" specimens

Figure 7. Instrumentation layout: LPs, LVDTs and reinforcement strain gauges ("sg") (a) and prestressed steel strips (in strengthened specimens "CAM1" and "CAM2") strain gauges (b).

3 ANALYSIS OF EXPERIMENTAL RESULTS

In this Section, the results of the experimental tests on the specimens described in Section 2 are analysed, first in terms of global drift-shear response of the subassemblages and corresponding observed damage evolution (Section 3.1), then in terms of local response of the joint panel, with corresponding shear stress-strain response (Section 3.2), and in terms of measured strain in steel reinforcement, for the beam longitudinal reinforcement, at beam/joint interface section, for stirrups of the reinforced, code compliant specimen, and for the external prestressed strips of the strengthened specimens. Finally, some remarks on the weight of the contributions corresponding to different deformation mechanisms to the total deformability of the subassemblages and on the observed dissipative capacity of the tested specimens are reported (Section 3.4).

3.1 Global response and damage evolution

In the following, the global response of the specimens is reported in terms of beam drift-versus-beam shear, with the beam drift calculated as the ratio between the displacement (imposed by the hydraulic actuator) at beam's end and the beam's length, L_b. This drift can be assumed as equal to the storey drift of the frame from which the subassemblage is ideally extracted. The beam shear-vs-drift responses of all tests are reported in Figure 8. In this Figure, the expected values of beam shear corresponding to flexural strength at yielding ($V_{b,y}$) and maximum ($V_{b,max}$) are reported, too, evaluated as the ratio between moments at yielding and maximum – calculated assuming a Mander et al.'s (1988) constitutive relationship for concrete (considering cover spalling and neglecting the effect of stirrups' confinement) and a Chang and Mander's (1994) elastic-plastic-hardening constitutive relationship for reinforcing steel – divided by the beam's clear length $L'_b=L_b-h_c/2$.

A comparison of tests' response envelopes is reported in Figure 8. Single beam shear-vs-drift responses are reported in Figure 9.

A detailed description of the observed damage with increasing imposed drift for all tests is reported in Tables 1 and 2. Photographic images of the observed damage at the end of test for all specimens are reported in Figure 10.

The as-built, unreinforced specimen 1NS showed the onset of joint cracking at 1%, followed by the attainment of the peak load, very close to the predicted beam flexural yielding, at 1.5%, and subsequently a rapid softening associated to the progress of the damage in the joint panel, up to the total collapse, with buckling of longitudinal reinforcement on the outer face of the joint panel, with test terminated at 6% drift, with a strength drop about equal to 40%. These observations, together with the data regarding the yielding of longitudinal beam reinforcement provided by strain gauges, that will be shown later (see Section 3.3), allow defining the response of this specimen as characterized by a "BJ-failure", i.e. a collapse of the subassemblage controlled by the failure of the joint panel following the flexural yielding of the beam.

The specimen 1S, with code-compliant transverse reinforcement in the joint panel, showed a ductile response, controlled by the development of a flexural plastic hinge at beam's end. The observed peak load was close to the predicted beam flexural strength. The test was terminated at 8% drift, with a strength drop about equal to 20%, caused by concrete cover spalling and buckling of longitudinal reinforcement in beam. In this specimen, only hairline cracking was observed in joint panel, at 1% drift as in specimen 1NS. Compared to specimen 1NS, a slightly higher strength is observed, thanks to post-yielding flexural hardening in beam, and, above all, a significantly delayed softening, leading to a clearly higher available ductility.

The strengthened specimen CAM1 showed a response very similar to the specimen 1S, with a ductile response controlled by the development of a flexural plastic hinge at beam's end, and a test terminated at 8% drift, with a softening caused by concrete cover spalling and buckling of longitudinal reinforcement in beam. Despite the absence of stirrups, only hairline cracking was observed in joint panel, slightly delayed compared to specimen 1S (i.e. at 1.5% drift instead of 1%), and apparently even less developed. Based on the observed damage, and the comparison of response envelopes (see Figure 9), the adopted solution resulted very effective in joint strengthening.

The strengthened specimen CAM2 showed an intermediate behaviour between 1NS and 1S, with an initially more developed flexural damage in beam and a significant delay in the development of damage in joint panel, compared to 1NS, but with a softening response controlled by the collapse of this element (with a total loss of integrity at the end of test) instead of a ductile response with a flexure-controlled collapse of beam element, as in specimen 1S. Apart from a slight lack of symmetry, likely due to an accidental difference between top and bottom concrete cover in beam, this intermediate behaviour is evident from the comparison of response envelopes, too (see Figure 8). The test was terminated at 8% drift, with a strength drop about equal to 50%.

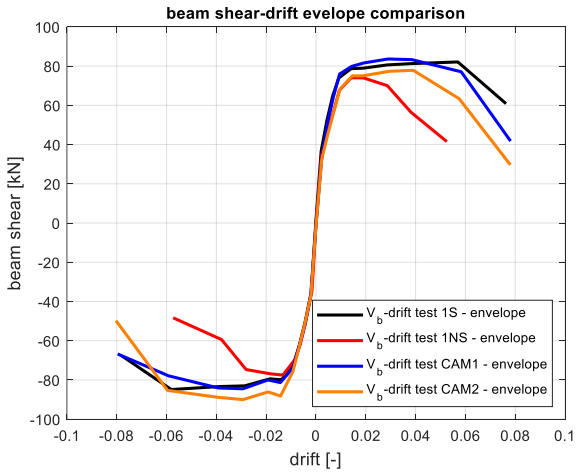

Figure 8. Comparison of tests' response envelopes.

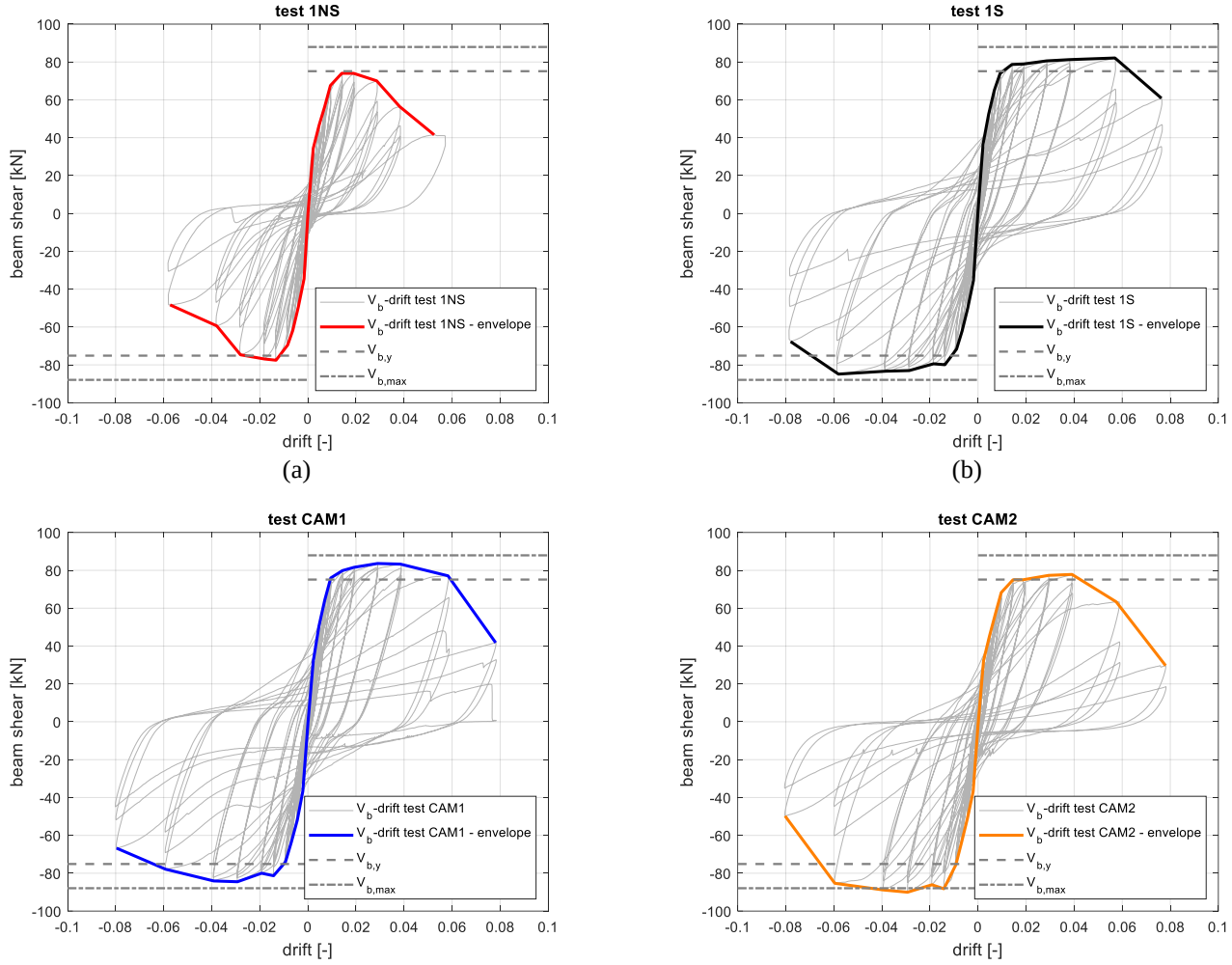

Figure 9. Beam shear-vs-drift response of tests 1NS (a), 1S (b), CAM1 (c), CAM2 (d).

Table 1. Observed damage for tests 1NS and NS.

Cycle #	Drift [%]	1NS	1S
1	0.25	No significant damage	No significant damage
2	0.5	Hairline cracking in beam at beam/joint interface	Hairline cracking in beam at beam/joint interface
3	0.75	Development of cracking in beam at beam/joint interface	Development of cracking in beam at beam/joint interface
4	1	Hairline cracking in joint panel	Hairline cracking in joint panel
5	1.5	Development of cracking in joint panel	Further development of cracking in beam at beam/joint interface
6	2	Further development of cracking in joint panel	"
7	3	Detachment of concrete cover on the outer face of the joint panel	"
8	4	Further detachment of concrete cover on the outer face of the joint panel	Visible detachment of concrete cover in beam
9	6	Buckling of longitudinal reinforcement on the outer face of the joint panel	Spalling of concrete cover and buckling of longitudinal reinforcement in beam
10	8	-	Fracture of longitudinal reinforcement in beam

Table 2. Observed damage for tests CAM1 and CAM2.

Cycle #	Drift [%]	CAM1	CAM2
1	0.25	No significant damage	No significant damage
2	0.5	Hairline cracking in beam at post-strengthening section	Hairline cracking in beam at beam/joint interface and post-strengthening section
3	0.75	Development of cracking in beam at post-strengthening section	Development of cracking in beam at beam/joint interface and post-strengthening section
4	1	Further development of cracking in beam at post-strengthening section	Hairline cracking in joint panel
5	1.5	Hairline cracking in joint panel	Development of cracking in joint panel and in beam at strengthening section
6	2	Further development of cracking in beam at post-strengthening section	Further development of cracking in joint panel and in beam at strengthening section
7	3	"	Further development of cracking in joint panel
8	4	Spalling of concrete cover	"
9	6	Buckling of longitudinal reinforcement in beam	Detachment of concrete cover on the outer face of the joint panel
10	8	Fracture of longitudinal reinforcement in beam	Buckling of longitudinal reinforcement on the outer face of the joint panel

(a) (b) (c) (d)

Figure 10. Observed damage at the end of test for tests 1NS (a), 1S (b), CAM1 (c), CAM2 (d).

3.2 *Local response: shear behaviour of joint panel*

The response of the joint panel in the tested specimens is analysed in this Section. This response is usually analysed in terms of shear stress-strain relationship, making reference to an ideal pure shear behaviour, and evaluating (i) the shear distortion of the panel from the local strain measurement data provided by the LPs placed on the panel, and (ii) the corresponding shear stress from equilibrium considerations, starting from the applied load (i.e. beam shear).

Note that four different values of the shear distortion can be calculated starting from LPs data, i.e. one for each "sub-triangle" of the instrumentation layout on the joint panel (see Figure 7a); more specifically, if ε_x is the horizontal strain (provided by LP jb or LP jt), ε_y the vertical strain (provided by LP jl or LP jr), and ε_θ the diagonal strain (provided by LP jd1 or LP jd2), the shear strain, γ_j, can be evaluated as:

$$\gamma_j = \frac{\varepsilon_\theta - \varepsilon_x \cos^2\theta - \varepsilon_y \sin^2\theta}{\sin\theta\cos\theta} \quad (3)$$

with θ representing the angle to the horizontal axis of the diagonals. Finally, the average of the four calculated values of γ_j (ε_{jb}-ε_{jl}-ε_{jd2}; ε_{jb}-ε_{jr}-ε_{jd1}; ε_{jt}-ε_{jl}-ε_{jd1}; ε_{jt}-ε_{jr}-ε_{jd2}) is evaluated.

The corresponding joint shear stress, τ_j, is calculated as the ratio between the horizontal joint shear, V_{jh}, and the horizontal joint area, A_{jh}, with V_{jh} calculated according to Eq. (2), for each step of the test, starting from the beam shear V_b, and assuming the tension in beam longitudinal reinforcement equal to $T = M_b/(0.9\cdot d) = (V_b\cdot L'_b)/(0.9\cdot d)$, i.e. estimating the internal lever arm as 0.9 times the effective depth, d:

$$\tau_j = \frac{V_{jh}}{A_{jh}} = \frac{1}{A_{jh}}\left(T - V_c\right) = \\ = \frac{1}{A_{jh}}\left(\frac{M_b}{0.9d} - \frac{V_b L_b}{2L_c}\right) = \frac{1}{A_{jh}}\left(\frac{V_b L'_b}{0.9d} - \frac{V_b L_b}{2L_c}\right) \quad (4)$$

Figure 11 reports the evolution, during the test, of the joint panel shear strain of the four specimens. For the specimen 1NS, data are reported until measurements provided by instruments were considered as reliable, compatibly with the damage to the joint panel. As reported in Tables 1 and 2, and described in Section 3.1, first visible cracking in joint panel was observed between 4th and 5th cycles, i.e. between 1% and 1.5%. As expected from damage observation, highest values are observed for specimens 1NS and CAM2. More specifically, for specimens 1S and CAM1 a relatively low shear distortion is observed, and, interestingly, more limited for CAM1 specimen compared to 1S. Moreover, note that in these specimens, approaching the end of test, a decrease in peak cycle values of shear strain is observed, particularly in the last (10th) cycle for specimen 1S and in the last two (9th and 10th) for specimen CAM1, i.e. when a global softening behaviour is observed, with decreasing load, the shear distortion decreases, too, and this is consistent with the fact that the response of the joint panel was not degrading, i.e. it did not control the global softening. On the contrary, a regular increase in shear strain is observed for 1NS and CAM2 specimens. Specifically, it is interesting to observe how the presence of the strengthening led this specimen to an intermediate behaviour, closer to CAM1 in the first cycles, and then with very significant shear strain values with progressing damage, but significantly delayed compared to specimen 1NS.

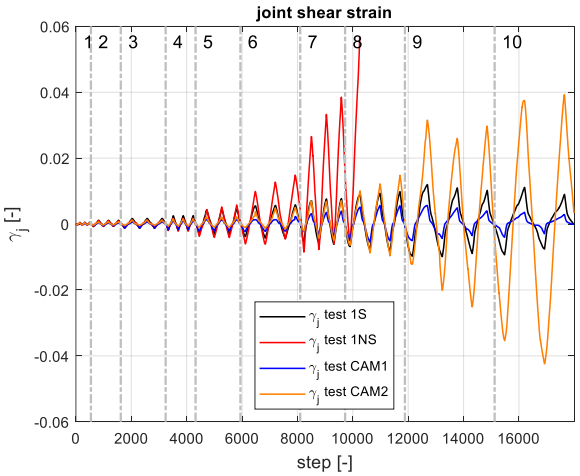

Figure 11. Evolution of joint panel shear strain during the test for all specimens (vertical grey dot-dashed lines separate imposed drift cycles).

The shear stress-strain response of the joint panel is reported, for all specimens, in Figure 12. The shear stress is normalized dividing it by the square root of the cylindrical compressive strength of concrete, $\tau_j/\sqrt{f_c}$. The specimen CAM1, compared to 1S, shows, given a very similar global response (and thereby a very similar evolution of the calculated $\tau_j/\sqrt{f_c}$), a higher initial stiffness in the $\tau_j/\sqrt{f_c}$ – γ_j relationship, as a consequence of a delayed and more limited cracking of the joint panel. In both cases, as highlighted previously, the envelope of the shear response of the joint panel does not show a softening behaviour, i.e. with decreasing load

(and $\tau_j/\sqrt{f_c}$), γ_j decreases, too. On the contrary, in specimens 1NS and CAM2, in which the evidence of the observed damage led to the conclusion that the failure of the joint element controlled the softening response of the subassemblage, the shear response of the joint panel confirms this observation, with a clear softening behaviour; a complete direct comparison between these two tests unfortunately is not possible, due to the interruption in data measurement in specimen 1NS caused by the damage to the joint panel.

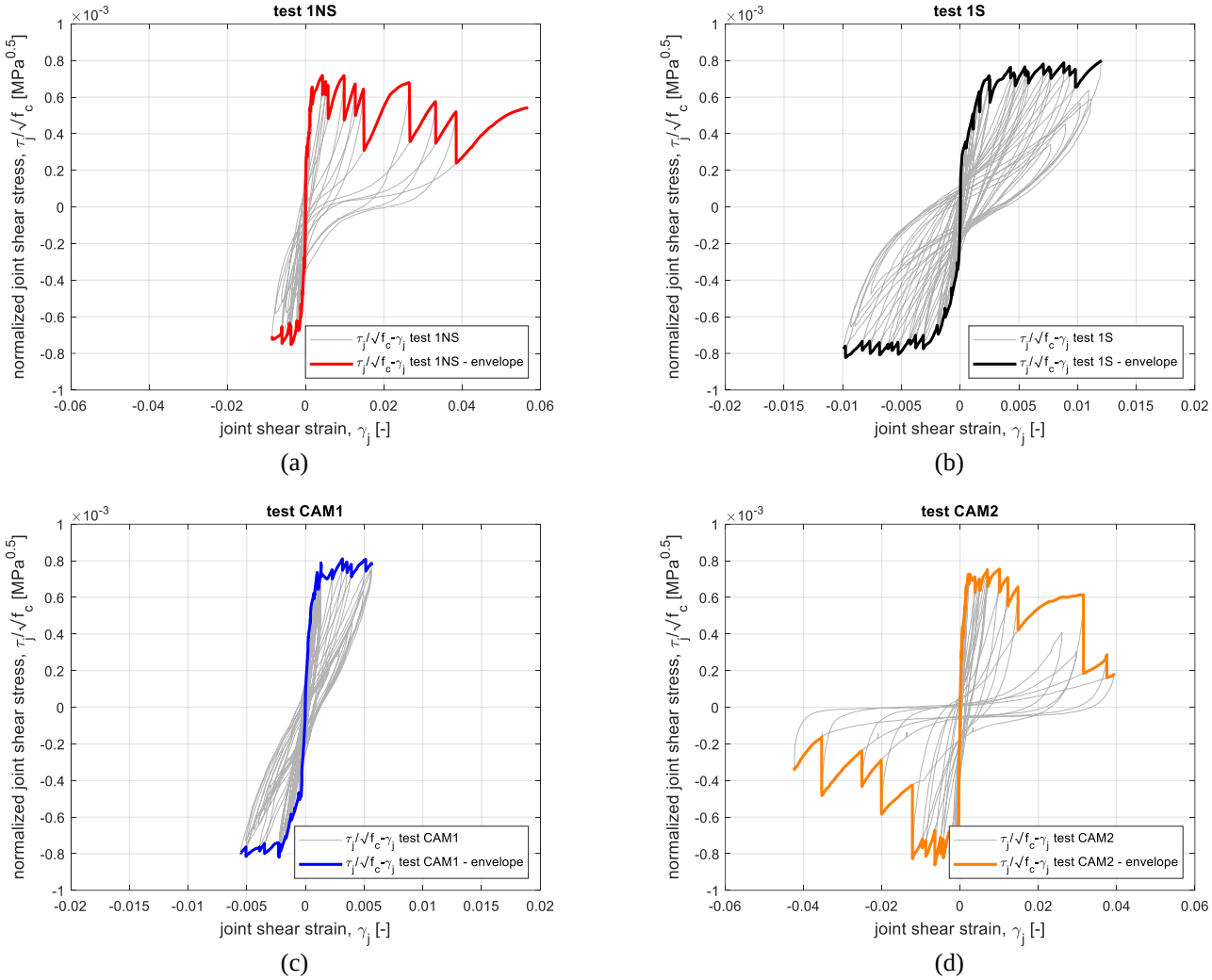

(a) (b) (c) (d)

Figure 12. Joint shear (normalized) stress-vs-strain response of tests 1NS (a), 1S (b), CAM1 (c), CAM2 (d).

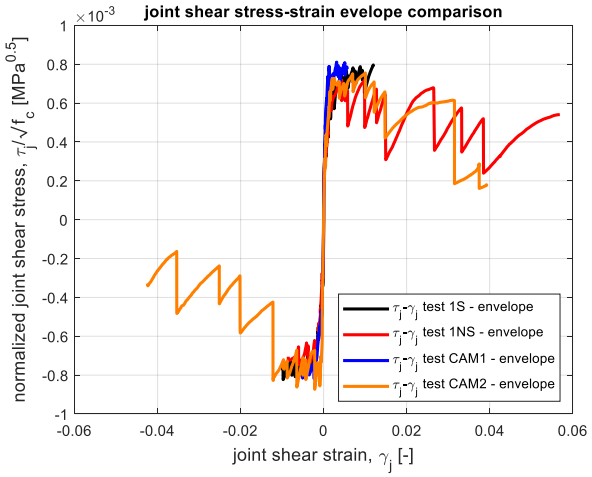

Figure 13. Comparison of joint shear (normalized) stress-vs-strain response envelopes.

A comparison of shear stress-strain response envelopes is reported in Figure 13.

3.3 Local response: strain of longitudinal reinforcement, stirrups and steel strips

In this Section, the evolution, during the tests, of the strain measured by strain gauges (see Figure 7) is illustrated and analyzed. These strain gauges were applied on beam longitudinal reinforcement at the beam/joint interface section in all specimens, on joint panel transverse reinforcement present in the reinforced specimen 1S, and on the prestressed steel strips in the strengthened specimens CAM1 and CAM2.

Figure 14 reports the evolution during the test of strain in bottom and top longitudinal reinforcement in beam at beam/joint interface (referring to the orientation of the specimens reported in Figure 6). The yielding strain of longitudinal reinforcement is reported, too. Note

that, due to technical problems, the data regarding the bottom reinforcement in specimen 1NS were not available. As observed, in all specimens the yielding can be identified approximately at the 4th cycle (1% drift), slightly delayed in specimens 1NS and CAM2 (especially in the former), characterized by a higher deformability due to joint damage.

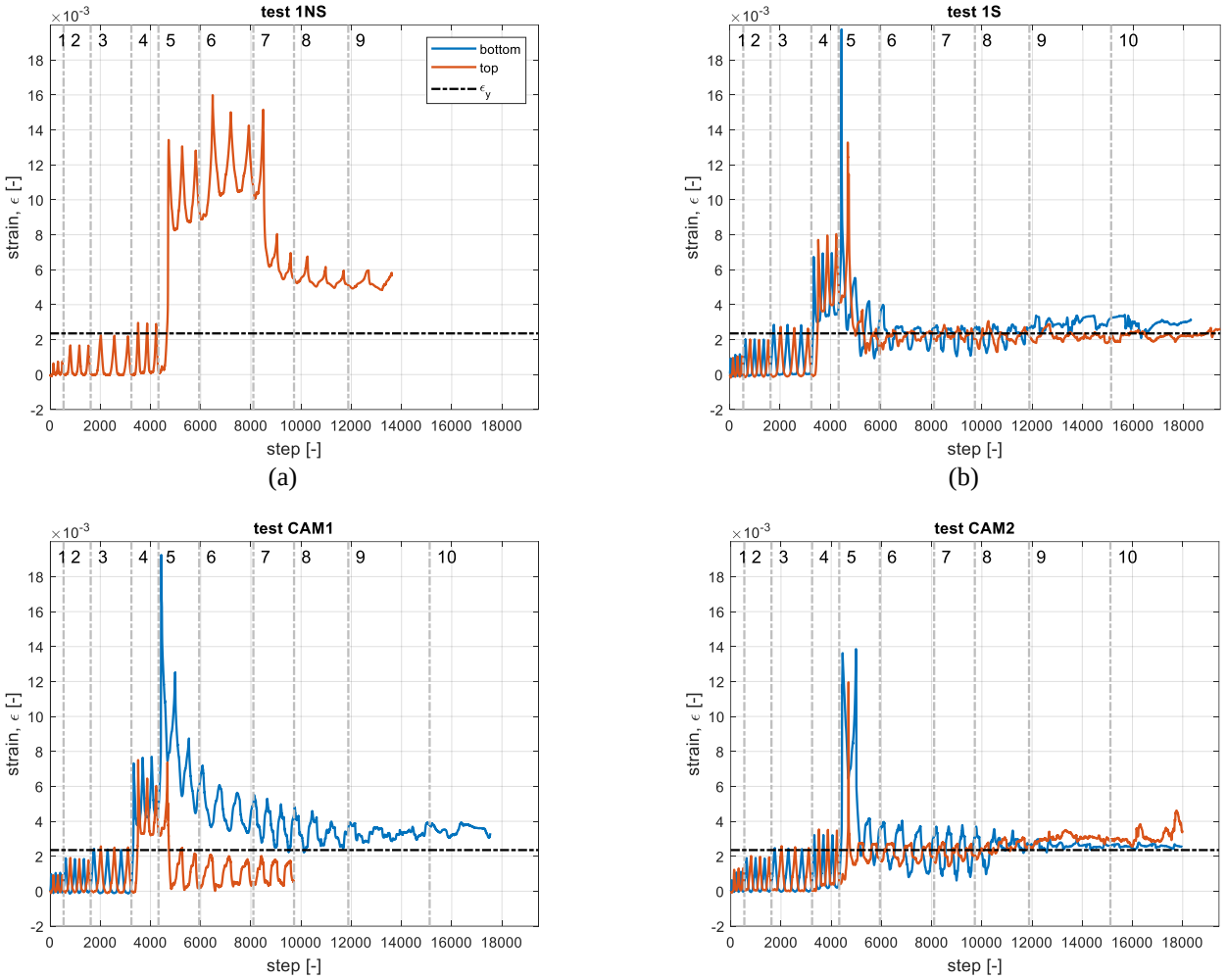

Figure 14. Evolution during the test (vertical grey dot-dashed lines separate imposed drift cycles) of strain in bottom and top longitudinal reinforcement in beam at beam/joint interface in tests 1NS (a), 1S (b), CAM1 (c), CAM2 (d).

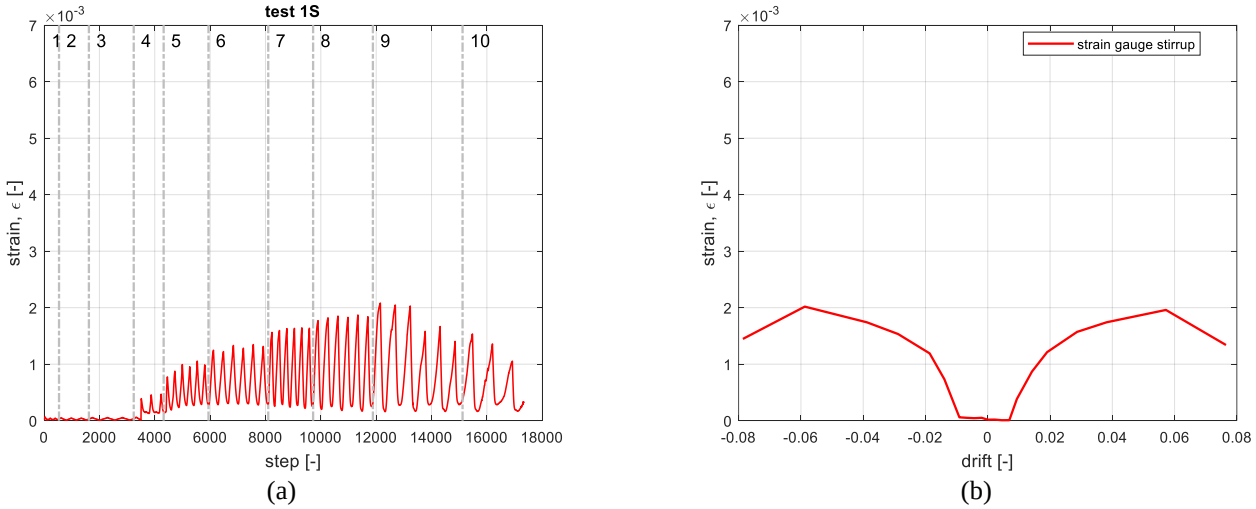

Figure 15. Strain in the mid-height stirrup located in the joint panel of specimen 1S: evolution during the test (vertical grey dot-dashed lines separate imposed drift cycles) (a) and values corresponding to first subcycles at maximum negative and positive imposed drift (b).

Figure 15 reports the strain in the mid-height stirrup located in the joint panel of specimen 1S. It is possible to observe that these measurements become significant during the 4th cycle (1% drift), consistent with the observed onset of visible cracking in the joint panel. Subsequently, this strain increases and, particularly from the 5th cycle on, with the development of the joint cracking along both panel diagonals, within each cycle local strain peaks are observed corresponding to maximum and minimum imposed drift. A decrease is observed in last cycle, as observed for the shear strain, consistently. Maximum values are close to 0.2%, i.e. below the yield strain. A more clear representation can be obtained reporting the strain corresponding to first subcycles at maximum negative and positive imposed drift, versus the corresponding drift values, see Figure 15b. In this Figure, as expected, a symmetric response is observed between positive and negative drift values, as well as the attainment of significantly increasing values starting from 1% drift, a progressive increase up to 6%, with increasing load, and, consistently, joint panel shear deformation (see Figure 11), and finally a decrease when the flexural damage to beam's end caused the global softening.

Figure 16 reports the strain in the prestressed steel strips of specimens CAM1 and CAM2. For the sake of brevity and clarity, only strain values of outer strips (N1, N2 and N3, see Figure 7b) – generally higher compared to inner strips – corresponding to first subcycles at maximum negative and positive imposed drift are reported. Note that in specimen CAM1, due to a technical problem, the initial strain value could not be reliably measured; hence, a value equal to 0.067%, corresponding to f_p = 120 MPa, was assumed. Figure 16a clearly shows that in specimen CAM1 for strips N1 and N3, up to a drift between 2% and 3%, the strain demand follows the sign of the imposed drift, consistent with the flexural demand at the end of the beam; this could be expected, since the strips, contrary to the stirrup in the specimen 1S, are anchored beyond the beam/joint interface section. Subsequently, with developing cracking in the joint panel, a strain increase with increasing imposed drift is observed, also if the strip is placed on the compressed side of the beam section. On the contrary, as expected, the response of the central strip N2 is roughly symmetric and characterized by higher strain values, in absolute terms, with developing cracking in the joint panel, as expected. For this strip, the attained strain values seem to indicate a non-negligible nonlinearity in the material response (see Figure 2b), with expected residual strain. Note that these strain values are higher than the strain values observed for the stirrup in specimen 1S, despite the lower shear strain observed in the joint panel, and this is consistent with the fact that in specimen CAM1 a prestress tension had to be overcome before crack opening.

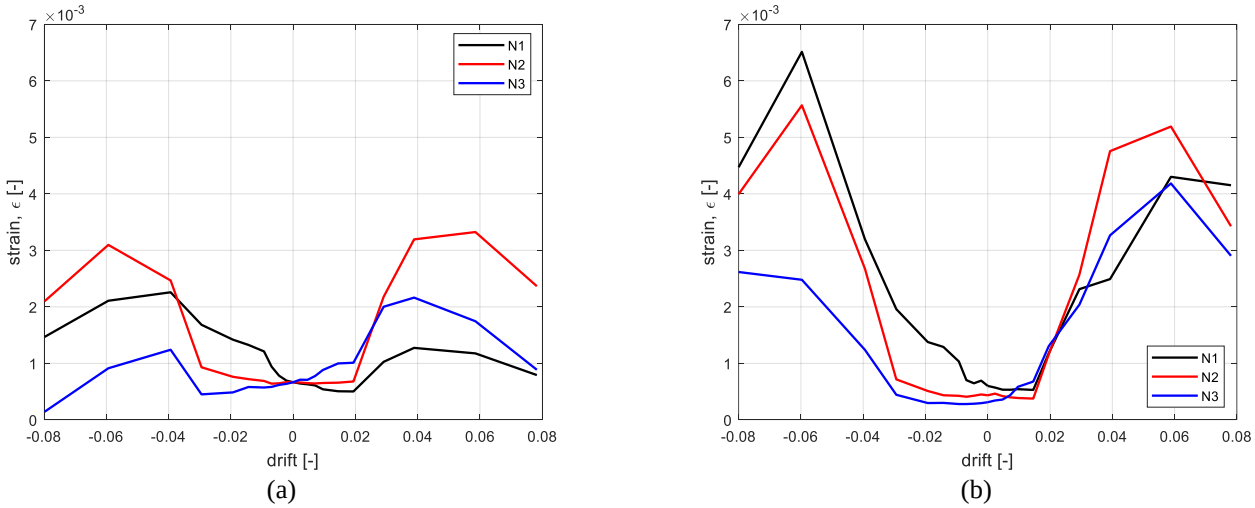

Figure 16. Strain in the prestressed steel strips of specimens CAM1 and CAM2: strain values of outer strips corresponding to first subcycles at maximum negative and positive imposed drift for specimen CAM1 (a) and CAM2 (b).

In the specimen CAM2, see Figure 16b, the attained strain values are significantly higher, highlighting a significant excursion in plastic field of the strips' material. A trend qualitatively similar to the one described for specimen CAM1 can be observed, but less regular when the damage became very significant, i.e. approximately from 4% drift on.

3.4 *Analysis of deformability contributions and hysteretic dissipative capacity*

Based on local deformation data, provided by instrumentation on joint panel and at beam's and columns' ends (see Figure 7a), it is possible to evaluate the contributions to the drift of the subassemblage corresponding to different deformation mechanisms, namely:

- shear strain in the joint panel, γ_j, reported in Section 3.2, whose contribution to the displacement at beam's end can be calculated as:

$$\Delta_{\gamma_i} = \gamma_i \cdot L_b^{'} - \gamma_i \cdot h_b \frac{L_b}{2L_c} \quad (5)$$

- end rotation in beam, θ_b, whose contribution to the displacement at beam's end can be calculated as:

$$\Delta_{\theta_b} = \theta_b \cdot L_b^{'} \quad (6)$$

- end rotation in bottom and top columns, θ_c^{bottom} and θ_c^{top}, whose contribution to the displacement at beam's end can be calculated as:

$$\Delta_{\theta_c} = \left(\theta_c^{bottom} + \theta_c^{top}\right) \cdot L_c^{'} \frac{L_b}{2L_c} \quad (7)$$

The remaining part should be attributed to the (mainly elastic) deformability of columns and beams, due to flexural (and, generally speaking, shear) deformability along these members. For further details, the reader is referred to (De Risi et al., 2016; Ricci et al., 2016; Verderame et al., 2018).

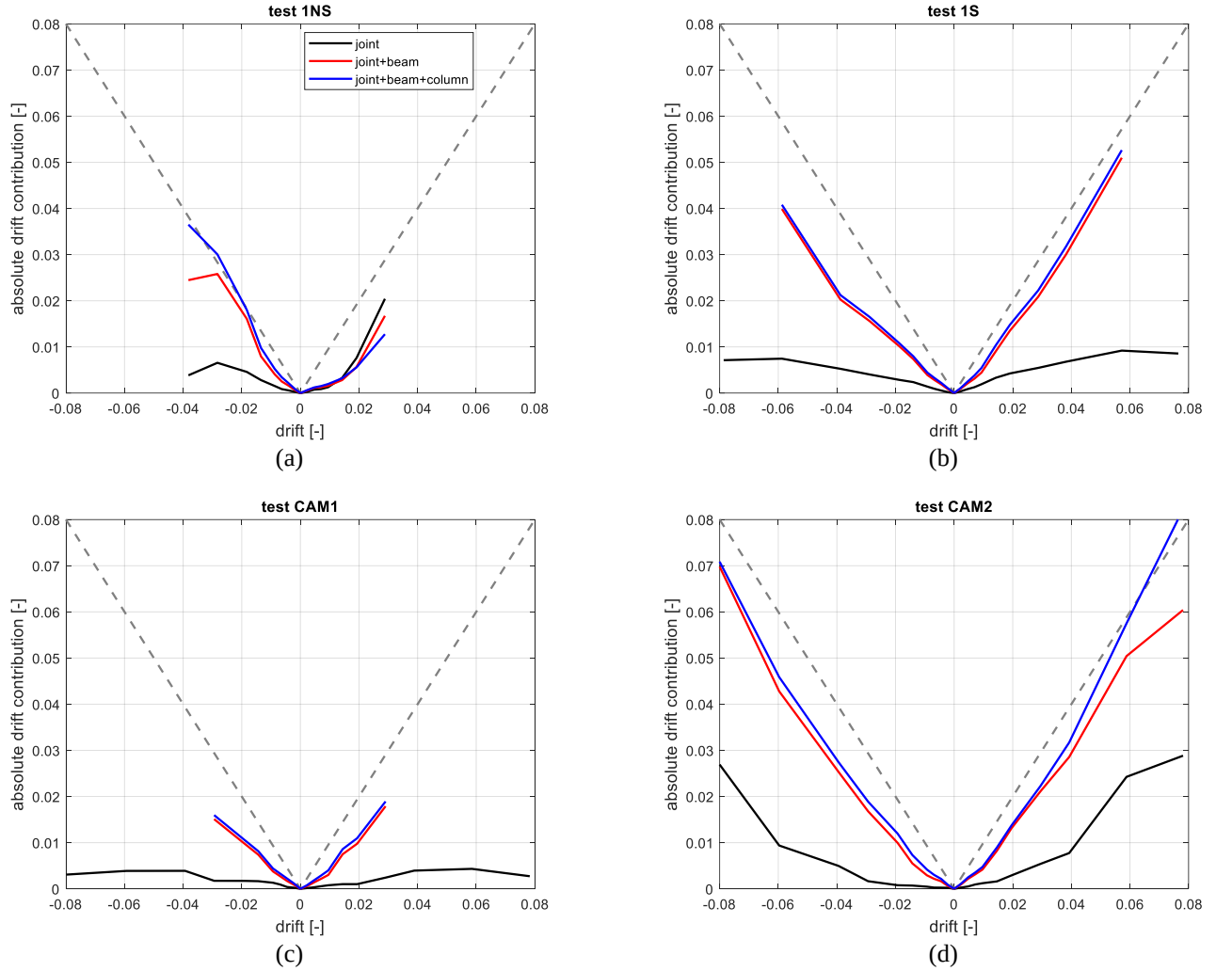

Figure 17. Drift contributions of different deformation mechanisms corresponding to first subcycles at maximum negative and positive imposed drift in tests 1NS (a), 1S (b), CAM1 (c), CAM2 (d).

Figure 17 reports the deformability contributions calculated according to the equations reported above for the four specimens, depending on the drift of the subassemblage. These contributions are not reported when data provided by instruments become not reliable because of significant damage. As shown, the deformability contribution corresponding to the rotation at columns' ends is generally significantly lower compared to the remaining

two, and this was expected, based on the observed collapse mechanisms. The deformability contribution corresponding to the shear deformation of the joint panel is clearly more significant if this element is more severely damaged, i.e. in specimen 1NS, for which, unfortunately, reliable data measurements stop quite early, and in specimen CAM2, especially when the damage to the joint panel becomes more significant, i.e. approximately from 4% drift on. In specimens that showed a flexure-controlled collapse, with ductile failure of beam, i.e. 1S and CAM1, the most significant deformability contribution corresponds to the beam element. In these specimens, the joint deformability contribution, relatively low, is however not negligible, and it is related to the cracking of the joint panel. This phenomenon is less developed, and thereby the corresponding deformability contribution too, in the specimen CAM1 compared to 1S.

Finally, it is interesting to evaluate the hysteretic energy dissipation capacity of the tested specimens. In this regard, the different collapse mechanisms and the consequent different weight of different deformation mechanisms to the total deformability of the subassemblage – as discussed above – are expected to influence the energy dissipation capacity, too (Verderame et al., 2018). The hysteretic energy dissipation capacity can be evaluated with reference to the well-known concept of "equivalent damping ratio", ξ_{eq}, see Eq. (8) (e.g. (Priestley, 2003)), with $E_{D,i}$ and $E_{So,i}$ representing the dissipated and strain energy, respectively, and the subscript "i" referring to the i-th subcycle of the experimental test.

$$\xi_{eq,i} = \frac{1}{4\pi}\frac{E_{D,i}}{E_{So,i}} \tag{8}$$

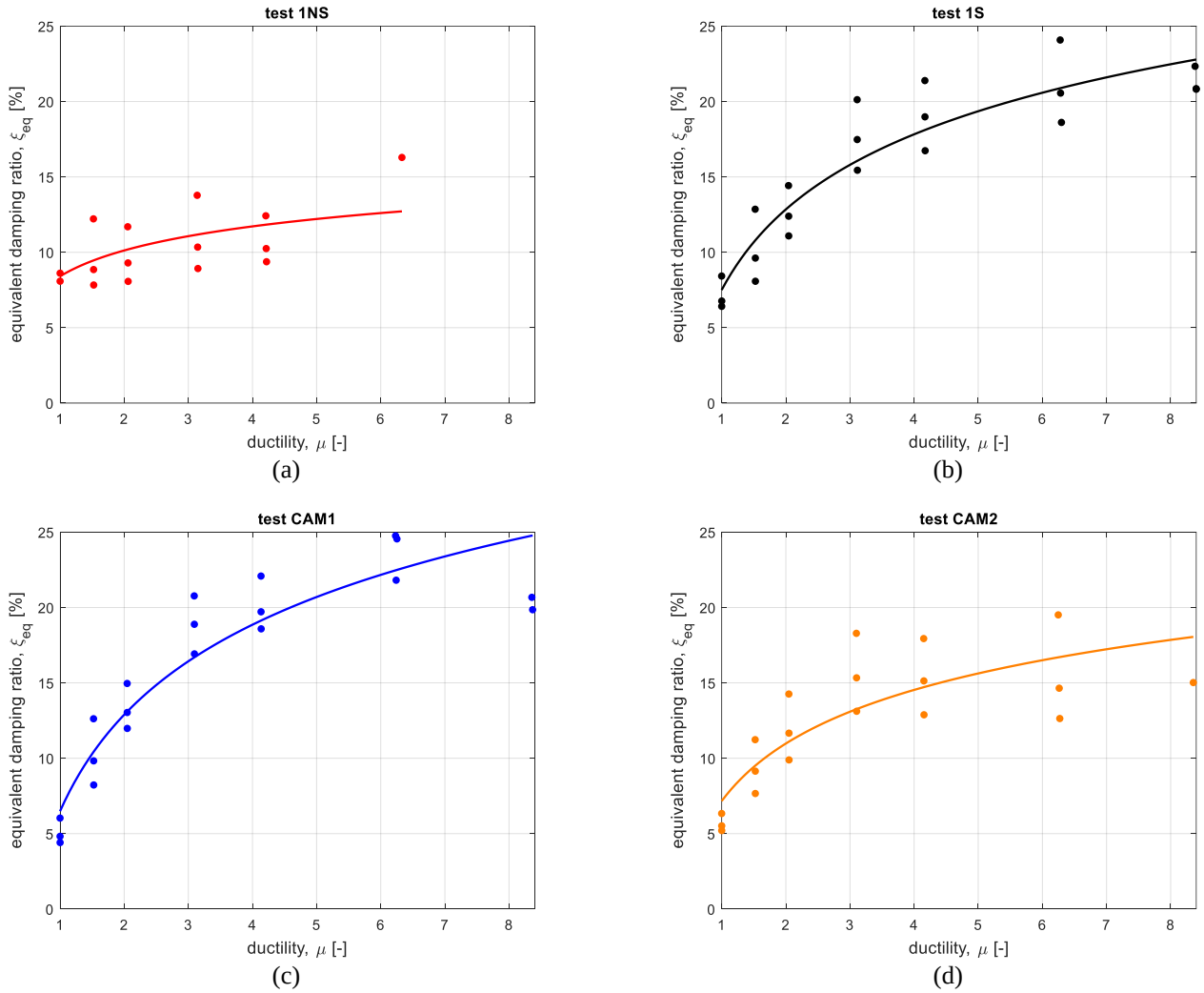

Figure 18. Equivalent damping ratio depending on displacement ductility and corresponding fitting functions for tests 1NS (a), 1S (b), CAM1 (c), CAM2 (d).

The calculated values of ξ_{eq} can be reported as a function of the ductility, μ, calculated as the ratio between the maximum imposed displacement of the i-th cycle and the maximum imposed displacement of the yielding cycle, that, with good approximation, can be assumed as

corresponding to the 4th cycle (1% drift). These values are reported as dots in Figure 18, for all the tested specimens. These reported values can be approximated by a fitting function, with a nonlinear least squares regression, assuming the functional form reported in Eq. (9) (Priestley, 2003).

$$\xi_{eq} = \xi_0 + a\left(1 - \frac{1}{\mu^{\beta}}\right) \quad (9)$$

Assuming $\beta = 0.1$ (Melo et al., 2015), the fitting functions reported as solid lines in Figure 18 are obtained. Figure 19 reports a direct comparison between these functions. As observed, the lowest dissipative capacity is shown by the specimen 1NS, characterized by an inelastic response controlled by the damage (up to complete collapse) of the joint panel. The specimens 1S and CAM1, characterized by a flexure-controlled collapse, with ductile failure of beam, show, on the contrary, the highest dissipative capacity. More specifically, the specimen CAM1, whose response, compared to the specimen 1S, is characterized by an even lower deformability contribution of the joint panel, shows a slightly higher dissipative capacity. This is consistent with the higher weight of a more dissipative deformation mechanism, i.e. the one corresponding to beam deformation (Verderame et al., 2018). Finally, the response of the specimen CAM2 is, again, intermediate between the response of flexure-controlled specimens 1S and CAM1 and specimen 1NS.

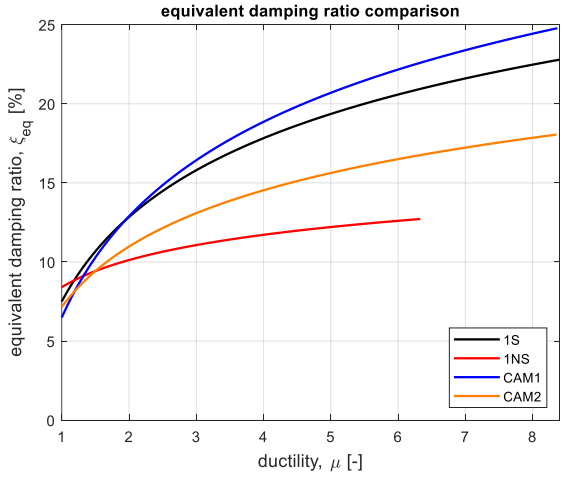

Figure 19. Comparison of fitted equivalent damping ratios.

4 CONCLUSIONS

In this study, results of experimental tests aimed at investigating the effectiveness of a strengthening approach based on the application of prestressed steel strips, using the CAM® technology, for unreinforced (i.e. without transverse reinforcement in the joint panel) external RC beam-column joints, representative of an existing, non-ductile RC building, have been presented and discussed. Two strengthening layouts have been tested, i.e. a "base solution" (CAM1) and second solution, based on a less invasive strengthening layout (CAM2). For reference purposes, one as-built, unreinforced specimen (1NS) and another one reinforced with code-compliant transverse reinforcement in the joint panel (1S) have been tested, too.

The main conclusions drawn from the observation and analysis of experimental results can be summarized as follows:

- The as-built, unreinforced specimens 1NS showed a collapse controlled by failure of the joint panel following beam yielding (i.e. a BJ-failure), leading to a significantly anticipated softening of the subassemblage;
- The code-complying reinforced specimen 1S showed a collapse controlled by ductile, flexure-controlled beam failure, showing only light cracking in the joint panel;
- The strengthened specimen CAM1 showed a collapse controlled by ductile, flexure-controlled beam failure, as in specimen 1S, thus demonstrating the effectiveness of the adopted strengthening solution, and showing an even slighter cracking in the joint panel;
- The strengthened specimen CAM2 showed an intermediate behaviour between 1S (or CAM1) and 1NS, i.e. an initial concentration of damage at beam's end, followed by the development of damage in the joint panel, significantly delayed with respect to 1NS specimen (and thereby leading to an overall higher available ductility), but anyway finally controlling the softening response, and the collapse mechanism, of the subassemblage.

These observations were confirmed by the analysis of local response data, that showed the higher shear deformation of the joint panel in specimen 1NS, as expected, the lowest in specimen CAM1, slightly less than in specimen 1S, and an intermediate behaviour of specimen CAM2, with a "delayed" shear deformation demand. Data provided by strain gauges placed on steel reinforcement highlighted the occurrence of beam flexural yielding in all specimens, and a strain demand in the joint transverse reinforcement of specimen 1S increasing with the

development of joint cracking, as for the prestressed steel strips of strengthened specimens CAM1 and CAM2, and, more specifically, significantly higher values for specimen CAM2, compared to CAM1, highlighting a significant nonlinearity in the response of the strengthening steel. Finally, the analysis of the deformability contribution of different deformation mechanisms confirmed the higher weight of beam deformability for specimens 1S and CAM1, and a different response, more influenced by joint deformability, for specimens 1NS and CAM2; consistently, the analysis of the (specific) hysteretic energy dissipation capacity showed a very similar – even slightly better – response of specimen CAM1 compared to 1S, the worst behaviour of specimen 1NS, and, again, the intermediate behaviour of specimen CAM2.

Future investigations will be focused on a deeper analysis of experimental data, regarding, for instance, local strain data on strengthening steel strips, aimed at assessing the applicability and the effectiveness of capacity models proposed by literature in evaluating the contribution of the adopted strengthening and predicting the collapse mechanisms actually observed.

ACKNOWLEDGEMENTS

This work was developed under the financial support of ReLUIS-DPC 2019-2021 – WP5: Interventi di rapida esecuzione a basso impatto ed integrati and WP11: Contributi normativi relativi a Costruzioni Esistenti in Cemento Armato, funded by the Italian Department of Civil Protection (DPC). EDIL CAM® Sistemi Srl provided the reinforcing materials and realized the strengthening interventions. These supports are gratefully acknowledged.

REFERENCES

Antonopoulos C.P., Triantafillou T.C., 2003. Experimental investigation of FRP strengthened RC beam-column joints. *Journal of Composites for Construction*, **7**(1), 39-49.

Celik O.C., Ellingwood B.R., 2008. Modeling beam-column joints in fragility assessment of gravity load designed reinforced concrete frames. *Journal of Earthquake Engineering*, **12**(3), 357-381.

CEN, 2004. European standard EN1992-1-1. Eurocode 2: Design of concrete structures - Part 1-1: General rules and rules for buildings. Comité Européen de Normalisation, Brussels.

CEN, 2005a. European Standard ENV 1998-1-1/2/3. Eurocode 8: design provisions for earthquake resistance of structures. Part 1: general rules. Technical Committee 250/SC8, Comité Européen de Normalisation, Brussels.

CEN, 2005b. European standard EN1998-3. Eurocode 8: Design provisions for earthquake resistance of structures. Part 3: Assessment and retrofitting of buildings. Comité Européen de Normalisation, Brussels.

Chang G.A., Mander J.B., 1994. *Seismic energy based fatigue damage analysis of bridge columns: Part 1 - evaluation of seismic capacity*. Technical Report NCEER-94-0006. National Center for Earthquake Engineering Research, State University of New York at Buffalo, Buffalo, NY, USA.

Circolare 2009. Circolare del Ministero dei Lavori Pubblici n. 617 del 2/2/2009. Istruzioni per l'applicazione delle "Nuove norme tecniche per le costruzioni" di cui al D.M. 14 gennaio 2008. G.U. n. 47 del 26/2/2009. (in Italian)

Circolare 2019. Circolare del Ministero dei Lavori Pubblici n. 7 del 21/1/2019. Istruzioni per l'applicazione dell'«Aggiornamento delle "Norme tecniche per le costruzioni"» di cui al decreto ministeriale 17 gennaio 2018. G.U. n. 35 dell'11/2/2019. (in Italian)

Clyde C., Pantelides C.P., Reaveley L.D., 2000. *Performance-based evaluation of exterior reinforced concrete buildings joints for seismic excitation*. PEER Report No. 2000/05. Pacific Earthquake Engineering Research Center, University of California, Berkeley, CA, USA.

De Risi M.T., Ricci P., Verderame G.M., 2017. Modelling exterior unreinforced beam-column joints in seismic analysis of non-ductile RC frames. *Earthquake Engineering and Structural Dynamics*, **46**(6), 899-923.

De Risi M.T., Ricci P., Verderame G.M., 2018. Empirical model of unreinforced beam-column RC joints with plain bars. *The Open Construction and Building Technology Journal*, **12**, 334-349.

De Risi M.T., Ricci P., Verderame G.M., Manfredi G., 2016. Experimental assessment of unreinforced exterior beam-column joints with deformed bars. *Engineering Structures*, **112**, 215-232.

De Risi M.T., Verderame G.M., 2017. Experimental assessment and numerical modelling of exterior non-conforming beam-column joints with plain bars. *Engineering Structures*, **150**, 115-134.

Decreto Ministeriale 14 febbraio 1992. Norme tecniche per le opere in c.a. normale e precompresso e per le strutture metalliche. G.U. n. 65 del 18/3/1992. (in Italian)

Decreto Ministeriale 24 gennaio 1986. Norme tecniche relative alle costruzioni antisismiche. G.U. n. 108 del 12/5/1986. (in Italian)

Del Vecchio C., Di Ludovico M., Balsamo A., Prota A., Manfredi G., Dolce M., 2014. Experimental investigation of exterior RC beam-column joints retrofitted with FRP systems. *Journal of Composites for Construction*, **18**(4).

Dolce M., Gigliotti R., Laterza M., Nigro D., Marnetto R., 2001a. Il rafforzamento dei pilastri in c.a. mediante il sistema CAM. *Atti del X Convegno ANIDIS "L'ingegneria sismica in Italia"*, September 9-13, Potenza-Matera, Italy. Paper F3-01. (in Italian)

Dolce M., Nigro D., Ponzo F.C., Marnetto R., 2001b. Rafforzamento delle strutture murarie: il sistema CAM di Cuciture Attive per la Muratura. *Atti del X Convegno ANIDIS "L'ingegneria sismica in Italia"*, September 9-13, Potenza-Matera, Italy. Paper E3-07. (in Italian)

Jeon J.S., Lowes L.N., DesRoches R., Brilakis I., 2015. Fragility curves for non-ductile rein-forced concrete

frames that exhibit different component response mechanisms. *Engineering Structures*, **85**, 127-143.

Jeon J.S., Shafieezadeh A., DesRoches R., 2014. Statistical models for shear strength of RC beam-column joints using machine-learning techniques. *Earthquake Engineering and Structural Dynamics*, **43**(14), 2075-95.

Karayannis C.G., Chalioris C.E., and Sirkelis G.M., 2008. Local retrofit of exterior RC beam–column joints using thin RC jackets – An experimental study. *Earthquake Engineering and Structural Dynamics*, **37**, 727-746.

Leonori M., Vari A., 2019. Cuciture attive a marchio CAM®. Applicazioni e calcolo su edifici in CA. EDIL CAM® Sistemi Srl. https://www.edilcamsistemi.com/allegati/strumenti/190313-Linee_guida_CA-REV12.pdf

Mander J.B., Priestley M.J.N., Park R., 1988. Theoretical stress-strain model for confined concrete. *ASCE Journal of Structural Engineering*, **114**(8), 1804-1826.

Masi A., Santarsiero G., Nigro D., 2013. Cyclic tests on external RC beam-column joints: role of seismic design level and axial load value on the ultimate capacity. *Journal of Earthquake Engineering*, **17**(1), 110-36.

Melo J., Varum H., Rossetto T., 2015. Cyclic behaviour of interior beam-column joints reinforced with plain bars. *Earthquake Engineering and Structural Dynamics*, **44**(9), 1351-1371.

NTC 2008. Decreto ministeriale 14 gennaio 2008 – Norme Tecniche per le Costruzioni. G.U. n. 29 del 4/2/2008. (in Italian)

NTC 2018. Decreto ministeriale 17 gennaio 2018 – Aggiornamento delle "Norme Tecniche per le Costruzioni". G.U. n. 42 del 20/2/2018. (in Italian)

Pantelides C.P., Hansen J., Nadauld J., Reaveley L.D., 2002. *Assessment of reinforced concrete building exterior joints with substandard details*. PEER Report No. 2002/18. Pacific Earthquake Engineering Research Center, University of California, Berkeley, CA, USA.

Park S., Mosalam K.M., 2012. Analytical model for predicting the shear strength of unreinforced exterior beam-column joints. *ACI Structural Journal*, **109**, 149-59.

Priestley M.J.N., 2003. *Myths and fallacies in earthquake engineering, revisited*. The Mallet Milne Lecture. IUSS Press, Pavia, Italy.

Priestley M.J.N., 1997. Displacement-based seismic assessment of reinforced concrete buildings. *Journal of Earthquake Engineering*, **1**(1), 157-192.

Ricci P., De Luca F., Verderame G.M., 2011. 6th April 2009 L'Aquila earthquake, Italy: Reinforced concrete building performance. *Bulletin of Earthquake Engineering*, **9**(1), 285-305.

Ricci P., De Risi M.T., Verderame G.M., Manfredi G., 2016. Experimental tests of unreinforced exterior beam-column joints with plain bars. *Engineering Structures*, **118**, 178-194.

Shafaei J., Hosseini A., Marefat M.S., 2014. Strengthening of substandard reinforced concrete beam-column joints by external post-tension rods. *Engineering Structures*, **81**, 265-288.

Spinella N., Colajanni P., Recupero A., 2014. Experimental in situ behaviour of unreinforced masonry elements retrofitted by pre-tensioned stainless steel ribbons. *Engineering Structures*, **73**, 740-753.

Thermou G.E., Elnashai A.S., 2006. Seismic retrofit schemes for RC structures and local-global consequences. *Progress in Structural Engineering and Materials*. doi:10.1002/pse.208

Verderame G.M., De Risi M.T., Ricci P., 2018. Experimental investigation of exterior unreinforced beam-column joints with plain and deformed bars. *Journal of Earthquake Engineering*, **22**(3), 404-434.

Wong H.F., 2005. *Shear strength and seismic performance of non-seismically designed RC beam-column joints*. PhD Thesis. Hong Kong University of Science and Technology, Hong Kong.

Yang Y., Xue Y., Wang N., Yu Y., 2019. Experimental and numerical study on seismic performance of deficient interior RC joints retrofitted with prestressed high-strength steel strips. *Engineering Structures*, **190**, 306-318.

Yurdakul O., Avsar O., 2016. Strengthening of substandard reinforced concrete beam-column joints by external post-tension rods. *Engineering Structures*, **107**, 9-22.